Research Square

Preprints are preliminary reports that have not undergone peer review.
They should not be considered conclusive, used to inform clinical practice,
or referenced by the media as validated information.

Sequentially Self-Assembled Supramolecular Nanocomplexes Enable Systemic Cas9 RNP Delivery and In Vivo Tumor Genome Editing

Takumi Matsuo
Institute of Science Tokyo
Yuto Honda
honda.y.aj@m.titech.ac.jp

Institute of Science Tokyo
Toshizumi Chino
Institute of Science Tokyo
Takahiro Nomoto
The University of Tokyo
Yuriko Osakabe
Institute of Science Tokyo
Yutaka Miura
Institute of Science Tokyo
Nobuhiro Nishiyama
Institute of Science Tokyo

Research Article

Keywords: CRISPR/Cas9, tannic acid, self-assembly, gene editing therapy, boronic acid, block copolymer.

Posted Date: July 3rd, 2026

DOI: https://doi.org/10.21203/rs.3.rs-9977199/v1

License: This work is licensed under a Creative Commons Attribution 4.0 International License.
Read Full License

Additional Declarations: No competing interests reported.

Abstract

In vivo genome editing with CRISPR–Cas9 ribonucleoproteins (RNPs) holds substantial therapeutic promise, yet rapid bloodstream clearance and the absence of delivery systems capable of systemic tumor targeting have hindered its clinical translation. Herein, a supramolecular ternary complex platform is reported in which Cas9/sgRNA RNPs are co-assembled with tannic acid (TA) and phenylboronic acid (PBA)-conjugated polymers through sequential self-assembly, producing ~ 30 nm core–shell ternary complexes that protect RNPs from enzymatic degradation and dissociate selectively at endosomal pH. Upon intravenous administration in subcutaneous tumor-bearing mice, these ternary complexes exhibit prolonged blood circulation and preferential tumor accumulation, achieving 37.2% gene editing at tumor sites compared with only 1.5% for free RNPs. The platform successfully knocks out previously undruggable oncogenes including mutant KRAS and polo-like kinase 1 (PLK1), markedly suppressing tumor growth *in vivo*. By integrating sequential supramolecular self-assembly with stimuli-responsive cargo release, this strategy establishes a generalizable framework for systemically administered *in vivo* CRISPR therapeutics.

1. Introduction

Clustered regularly interspaced short palindromic repeat (CRISPR)-associated protein 9 (Cas9) nuclease systems have been established as a revolutionary gene editing tool with vast potential in biomedicine [1–4] and agriculture [5]. Among the available formats, the direct delivery of preformed Cas9/single-guide-RNA (sgRNA) ribonucleoprotein (RNP) complexes is uniquely attractive because it bypasses transcription and translation, enables rapid genome editing, and minimizes off-target activity compared with plasmid-DNA, mRNA, or AAV-based approaches [6],[7, 8]. These properties have motivated therapeutic development against cancer [9], diabetes [10], and muscular dystrophy [11].

Despite this promise, the clinical translation of RNP-based therapeutics has been hindered by two intrinsic barriers. First, the ~ 12 nm size and slightly anionic surface of RNP complexes severely limit cell-membrane translocation and nuclear import. Second, as bacteria-derived assemblies, RNPs are highly susceptible to enzymatic degradation by RNases and proteases in the bloodstream, abolishing editing activity within minutes of intravenous administration. Cationic lipid nanoparticles [12–14], gold nanoparticles [15–17], and hyaluronic-acid-based carriers [18] have therefore been engineered to encapsulate RNPs and improve cytosolic delivery. However, most of these systems lack precise control over intracellular release and exhibit insufficient blood retention for systemic targeting; consequently, the majority of *in vivo* studies have relied on local injection or hepatic accumulation[14]. Critically, few studies have established a quantitative correlation between pharmacokinetic profiles and on-site editing efficiency, an unmet need that has constrained the rational design of systemic RNP carriers and delayed clinical approval of *in vivo* CRISPR therapeutics.

To address these challenges, we previously reported a systemically applicable, protein-loaded ternary nanocomplex formed by sequential self-assembly of cargo proteins with tannic acid (TA, Fig. 1A) and

phenylboronic acid (PBA)-conjugated polymers(Fig. 1B) in aqueous media [19]. TA is a biodegradable and biocompatible polyphenol bearing multiple galloyl groups that engage proteins, viral capsids, and peptides through hydrogen bonding and hydrophobic interactions[20],[21]. The same galloyl groups also form reversible boronate esters with PBA side-chain residues at physiological pH (7.4) but readily dissociate under endosomal acidity (pH ~ 5.5) [22, 23]. This TA-boronate chemistry yields core–shell ternary nanocomplexes that exhibit prolonged blood circulation [24], preferential tumor accumulation [19, 25], and acid-triggered cargo release with high spatiotemporal selectivity. To date, however, the platform has been validated only with native cargo proteins; whether it can preserve the structural integrity and *in vivo* editing competence of the much larger and enzymatically fragile Cas9 RNP has remained an open question.

In this study, we extend the supramolecular ternary complex platform to the systemic delivery of Cas9 RNPs and demonstrate, to our knowledge for the first time, a quantitative pharmacokinetics–editing relationship for an RNP carrier in a solid-tumor model (Figs. 1C,D). The resulting ~ 30 nm RNP/TA/PBA-polymer ternary complexes exhibit prolonged blood circulation and preferential tumor accumulation following intravenous administration, achieve endosomal-pH-triggered RNP release, and reach 37.2% gene-editing efficiency at the tumor site versus 1.5% for free RNP. Leveraging this efficiency, we knock out previously undruggable oncogenes including mutant KRAS and polo-like kinase 1 (PLK1), markedly suppressing tumor growth *in vivo*. Together, these results establish a generalizable supramolecular framework for systemically administered *in vivo* CRISPR therapeutics that overcomes the tissue-targeting limitations of conventional RNP delivery systems.

2. Materials and Methods

Materials and methods to synthesize polymers were described in the Supplement information.

2.1. Cells and animals. The HeLa-Luc cell line was obtained from Caliper Life Science (Hopkinton, MA, USA). The cells were cultured in E-MEM supplemented with 10% FBS and 1% penicillin-streptomycin at 37 °C in a humidified atmosphere with 5% CO_2. HCT116 cell line was purchased from ATCC (Manassas, VA) and were cultured in McCoy's 5a Medium with 10% FBS and 1% penicillin-streptomycin at 37 °C in a humidified atmosphere with 5% CO_2. BALB/c nude mice (Four-week-old, female) were purchased from Japan SLC, Inc. (Hamamatsu, Japan). All animal experiments were reviewed, authorized, and conducted in accordance with the Guidelines for the Care and Use of Laboratory Animals established by the Animal Care and Use Committee of Tokyo Institute of Technology (Approval No. 2020-049).

2.2. Preparation of Cas9 protein and sgRNA (RNP) complex. The Cas9 protein (15 μg/μl) and the sgRNA were mixed in the equal molar ratios in D-PBS(-) and subsequently incubated at room temperature for 10 min according to a manufacturer's protocol of Synthego Co. Ltd. The sgRNA was used in a previous study for Luc gene editing[14]. The mixture was ultrafiltrated against D-PBS(-) using a 10 kDa molecular weight cut-off (MWCO) membrane (Millipore, Burlington, MA, USA) to remove the original glycerol-containing solution. The RNP complex comprising Cas9-GFP and sgRNA was prepared in the same

manner. The RNP solution was diluted to the designated concentration by D-PBS(-) or 10 mM HEPES for following experiments.

2.3. Preparation of RNP/TA complexes. TA was dissolved in D-PBS(-) at various concentrations to prepare TA solution. The TA and RNP solutions (750 nM) were mixed at a 1:1 volumetric ratio to achieve various [TA]/[RNP] molar ratios, followed by incubation for 10 min at room temperature.

2.4. Turbidity measurement of RNP/TA complex solution. As turbidity, the derived count rate of the RNP/TA complex solution (RNP: 750 nM) was measured using the Zetasizer Nano ZS (Malvern Instruments, Worcestershire, UK) following our previous study [19] at a detection angle of 173°.

2.5. Dynamic light scatter measurement. We monitored the hydrodynamic diameters of the RNP samples ([RNP] = 750 nM) in D-PBS(-) utilizing a Zetasizer Ultra Red instrument (Malvern Instruments, Worcestershire, UK). Dynamic light scattering (DLS) data were collected at a scattering angle of 173° and analyzed through cumulant analysis. For each sample, 10 consecutive runs were recorded at room temperature, with an acquisition duration of 5 seconds.

2.6. Preparation of RNP/TA/PBA-conjugated polymer ternary complexes. PBA-conjugated polymers (P[Glu(DET)/Glu(FPBA)] and P[Lys/Lys(FPBA)]) (1.0 mg/mL) aqueous solution was prepared in D-PBS(-). The RNP/TA complex ([TA]/[RNP]) = 30) was mixed with the PBA-conjugated polymer solution at the molar ratios of the polymer to RNP ([Polymer]/[RNP] ratios) of 30 , followed by a 10-min incubation at room temperature. In the *in vivo* experiment, the [Polymer]/[RNP] ratios of the ternary complex were set to 600.

2.7. Size analysis using FCS. Fluorescence correlation spectroscopy (FCS) measurements were conducted to assess the hydrodynamic sizes of the complexes, utilizing an LSM710 confocal laser scanning microscope (CLSM; Carl Zeiss, Oberkochen, Germany) featuring a ConfoCor module. The optical setup included a 488-nm argon laser for sample excitation and a 500–550 nm bandpass filter for signal collection. Aliquots of the prepared RNP samples (Cas9-GFP in D-PBS(-), [Cas9-GFP] = 200 nM) were transferred to an eight-well chamber. Measurements comprised 10 individual 10-s runs at room temperature. The Stokes–Einstein equation, calibrated against a rhodamine 6G standard, was applied to derive the hydrodynamic diameter from the determined diffusion coefficients. Additionally, the particle amplitude (AMPs) within the focal volume was monitored to calculate the number of RNP molecules loaded within each complex using the following equation:

All measurements were conducted under identical optical alignment and fluorescence conditions to ensure consistent observation volume and detection efficiency. Note that, this calculation provides an average loading value, rather than indicating that every individual nanoparticle strictly contains one RNP molecule. To evaluate complex stability, we utilized D-PBS(-) enriched with FBS (10–50% [v/v]) as the incubation medium. Concurrently, the pH-responsive behavior of the RNP ternary complexes was

investigated by monitoring their hydrodynamic sizes across a range of buffering conditions, including D-PBS(-) at pH 7.4, 50 mM HEPES buffer at pH 6.8, and 50 mM 2-morpholinoethanesulfonic acid (MES) buffer at pH 6.0 and 5.5.

2.8. TEM observation. A 3-μL sample of the RNP solution ([RNP] = 1 mM) prepared in 1 mM HEPES (pH 7.4) was applied to a carbon-supported copper grid (200 mesh) and allowed to dry under vacuum. Transmission electron microscopy (TEM) imaging was then conducted using a JEM-1400 system (JEOL, Tokyo, Japan) at an accelerating potential of 100 kV.

2.9. Agarose gel electrophoresis. The RNP formulations ([Cas9] = 1.1 μg per sample in D-PBS(-)) were electrophoresed on a 1% agarose gel at 100 V for 20 min, followed by band visualization using Coomassie Brilliant Blue (CBB) Stain One.

2.10. FBS degradation stability. RNP samples (100 nM) were incubated with 0, 10, and 50 % FBS in PBS at 37 °C for 24 hours. The samples (4 μg of Cas9) were loaded in 1 % agarose gel and electrophoresed at 100 V for 20 min, followed by band visualization using SYBR® Green □ Nucleic Acid Gel Stain.

2.11. RNase degradation stability. RNP samples (100 nM) were incubated with 1.0 mg/mL RNase at 37 °C for 2 hours. The samples (4 μg of Cas9) were loaded in 1 % agarose gel and treated at 100 V for 20 min. The bands were visualized using SYBR® Green □ Nucleic Acid Gel Stain.

2.12. Apparent binding constants of PBA-conjugated polymers with gallic acid (GA). Theapparent binding constants of PBA-conjugated polymers with GA were evaluated using ARS, following our previous study [19,22]. The fluorescent intensity of the ARS/PBA-conjugated polymer complexes was measured with fluorophotometer (Spark, TECAN, Zürich, Switzerland) at various concentrations of GA. The apparent binding constants were calculated under the assumption that a GA molecule would form a boronate ester with an FBPA molecule in polymers.

2.13. Zeta-potential measurement of TA/PBA-conjugated polymer. Zeta-potential measurement of the TA/PBA-conjugated polymer complex (TA: 100 μM, PBA-conjugated polymer: 100 μM) in 10 mM HEPES was performed using a Zetasizer Nano ZS with a folded capillary zeta-potential cell (DTS1070, Malvern Instruments). The measurement was repeated 10 times.

2.14. Subcellular distribution. HeLa-Luc cells were seeded on an eight-well chamber (1.0×10^4 cells/well) and incubated for 24 hours. The culture medium was replaced with fresh medium after a D-PBS(-) wash, and the cells were exposed to the RNP formulations (Cas9-GFP, [RNP] = 60 nM) for a 24-h incubation period. Organelle and nuclear staining were performed sequentially: the cells were first washed and incubated with 1 μM LysoTracker Red DND-99 for 30 min, and then treated with 16.2 μM Hoechst 33342 (Life Technologies, Carlsbad, CA, USA) for 3 min, with thorough D-PBS(-) rinses between each step. Confocal imaging was conducted in fresh D-PBS(-) using the LSM710 system, where excitation wavelengths were set at 488 nm (Cas9-GFP), 561 nm (LysoTracker Red), and 405 nm (Hoechst 33342). Subcellular distribution of RNP ternary complexes containing Cas9-GFP and Alexa647-labelled

polymers were observed in the similar manner, and the Pearson correlation coefficient was calculated by the ZEN software (Carl Zeiss).

2.15. Cellular uptake evaluation. HeLa-Luc cells, initially cultured in 96-well plates (1.0×10^4 cells/well) for 24 h, were washed with D-PBS(-) and treated with the RNP samples (Cas9-GFP, [RNP] = 30 nM) in 100 μL of medium. Following a 24-h incubation, the cells were washed with D-PBS(-), isolated via enzymatic dissociation with 50 μL of trypsin, and recovered in 150 μL of culture medium. Cell-associated Cas9-GFP fluorescence was analyzed using a Guava easy-Cyte 6-2L flow cytometer (Merck Millipore, Billerica, MA, USA) with the optical configuration set at Ex/Em = 488/525 nm.

2.16. *In vitro* Luc gene knockout study. We inoculated HeLa-Luc cells into 96-well plates at an initial density of 3.0×10^3 cells per well and cultured them for 24 h. Following a brief rinse with D-PBS(-), the cells were exposed to the RNP complexes ([RNP] = 30 nM) in 100 μL of culture medium for 72 h. To determine cellular viability, the incubation medium was refreshed, and the cells were maintained for 1 h in 110 μL of medium supplemented with 10% CCK-8 solution. Optical density at 450 nm was then recorded using a microplate reader. Subsequently, the cells were washed twice using D-PBS(+) and lysed via a 15-min incubation in 50 μL of a cell lysis buffer. Aliquots of the resulting lysate (20 μL) were transferred to a clean 96-well plate, and bioluminescence was quantified via a Luciferase Assay System using a GloMax 96 Microplate Luminometer (Promega Co., USA).

2.17. Western blot to detect Luc expression *in vitro*. To assess protein expression, the treated HeLa-Luc cells were rinsed twice with D-PBS(-) and harvested in 50 μL of a cell lysis buffer. Protein samples (20 μg per lane) were separated using 4–15% Mini-PROTEAN® TGX™ Precast Protein Gels (Bio-Rad, Hercules, CA, USA) under a TGS buffer system and transferred onto PVDF membranes. The membranes were blocked in 5% BSA/TBS-T for 1 h and washed before overnight incubation at 4 °C with an anti-Firefly Luc antibody (1:1,000; Abcam) or an anti-β-actin antibody (1:6,000; Abcam) prepared in an immunoreaction enhancer reagent (TOYOBO, Osaka, Japan). Following three washing cycles with TBS-T, the blots were incubated with an HRP-conjugated anti-rabbit secondary antibody (1:10,000; Cell Signaling). Protein bands were subsequently visualized via chemiluminescence using SuperSignal™ West Dura Extended Duration Substrate (Thermo Fisher Scientific) and analyzed with a Bio-Rad imaging system. These molecular weights were determined using a protein standard marker (Precision Plus Protein Dual Color Standards, #1610374, Bio-Rad), as in the following experiment.

2.18. *In vitro T7E1* study. HeLa-Luc cells (3.3×10^3 cells/well) were seeded into 96-well plates and incubated for 24 hours. The cells were washed with D-PBS(-) and incubated with RNP samples (RNP: 30 nM) in 100 μL of the medium for 72 hours. After washing with D-PBS(-), 50 μL of trypsin-EDTA was added and incubated for 5 minutes to detach the cells. After washing the cells with D-PBS(-), the cells were resuspended with 50 μL of Cell Culture Lysis and incubated with 2 μL of Proteinase K following steps: 65°C for 15 min, 95°C for 10 min. The lysate was purified using QIAquick PCR Purification Kit (Qiagen) following the manufacture protocol. The target genomic regions were amplified via PCR under the following conditions: 94 °C for 30 s; 35 cycles of 98 °C for 15 s, 66 °C for 25 s, and 68 °C for 70 s;

followed by 68 °C for 30 s, and holding at 4 °C. The PCR products were purified utilizing QIAquick PCR Purification Kits, and 400 ng of the isolated DNA was introduced into a 15-μL reaction volume containing 1× NEBuffer 2. Heteroduplex formation was driven by a controlled thermal annealing sequence: initial denaturation at 95 °C for 5 min, gradual cooling to 85 °C (ramp rate: -2 °C/s) and subsequently to 25 °C (ramp rate: -0.1 °C/s), and a final maintenance step at 4 °C. The matrix was then incubated with 1 μL of Resolvase (Takara Bio, Shiga, Japan) at 37 °C for 15 min to cleave mismatched sites. The resultant DNA fragments were analyzed by 1% agarose gel electrophoresis with SYBR™ Green I visualization. All primer sequences utilized in this T7E1 assay are summarized in Table S3.

2.19. *In vitro* Luc DNA cleavage assay.The Luc target region DNA was extracted, following the protocol of *in vitro T7E1* study.The extracted Luc target region DNA with 300 ng was incubated with RNP samples (30 pmol) in D-PBS(-) pH 7.4 or 50 mM MES buffer pH 5.5 for 60 min at [RNP]/[TA]/[PBA-conjugated Polymer] = 1/50/250. After the incubation, the reaction solution was mixed with 50mM Tris buffer (pH8.0) at 1/1(vol/vol) for neutralization. The mixture was isolated by agarose electrophoresis with DNA Ladder followed by SYBR safe staining to visualize DNA bands.

2.20. Biodistribution of the RNP ternary complex. For evaluation of the biodistribution, fluorescently labelled sgRNA was prepared using Label IT® Cy5 Labeling kit (Mirus Bio LLC, Madison, WI, USA) according to the manufacturer's protocol. The sgRNA and the labelling reagent were mixed at the molar ratio of 1.00 and 0.25, respectively. A subcutaneous HeLa-Luc tumor model was prepared by inoculating HeLa-Luc cells into the right back of BALB/c nude mouse (5.0×10^6 cells/mouse) subcutaneously. RNP samples containing Cy5 labelled sgRNA were intravenously injected to the mouse intravenously at an RNP dose of 38.4 μg (32.0 μg of Cas9 and 6.4 μg of sgRNA)/mouse. At 1- and 10-hours post-injection, blood with 20 μL was collected from right tail vein. Furthermore, the mice were euthanized, and the organs were removed and washed using saline at 2-, 6-, and 24-hours post-injection,. The harvested organs and blood were mixed with passive lysis buffer, followed by homogenization and centrifugation (10,000 × g, 10 min, 4 °C). The collected supernatants were then placed into black 96-well plates, where Cy5 fluorescence was measured with a Spark microplate reader (*Ex*/*Em*: 650/667 nm).

2.21. *In vivo* Luc gene knockout study. Hela-Luc cells were subcutaneously inoculated into the back of BALB/c nude mouse (4.0×10^6 cells/mouse) for the preparation of subcutaneous HeLa-Luc tumor models. When the tumor volume reached approximately 150 mm^3, RNP samples were injected to the mouse intravenously at an RNP dose of 38.4 μg/mouse. Luc activity on tumor was measured 13 minutes after intraperitoneal injection of luciferin using *in vivo* imaging system (IVIS, Perkin Elmer, Waltham, MA, USA) on 0 day before sample injections, and 3 days and 7 days after sample injections. At 7 days post-injection, the tumors were collected from the sacrificed mice, which was mixed with passive lysis buffer. After the homogenization, the luminescence intensities were measured using a Luciferase Assay System by Lumat LB9507 (Berthold Technologies, Bad Wildbad, Germany).

To detect the indels in the Luc gene, HeLa-Luc cells (4.5×10^6 cells/mouse) were injected subcutaneously on the back flank of BALB/c nude mouse. Upon attaining a tumor volume of

approximately 150 mm^3, mice received intravenous injections of RNPs via the tail vein at a dosage of 38.4 μg/mouse on days 0, 2, and 4. The tumor tissue was harvested on day 16, and genomic DNA was extracted using DNeasy Blood & Tissue Kit according to the manufacturer's instructions. Then, the targeted gene sequence was amplified using the following PCR amplification program (98 °C for 2 min; (98 °C for 10 s; 60 °C for 15 s; 68 °C for 1 min) for 35 cycles; 68 °C for 30 sec and then keep at 4 °C). After purification, the amplicons were sent to the sanger sequencing (Reaction: Dye Terminator ver 3.1 (Applied Biosystems), Analysis: Genetic Analyzer 3730xl DNA Analyzer, (Thermo Fisher Scientific). The result was analysed using TIDE application.

2.22. Western blot to detect Luc expression *in vivo*. RNP samples were intravenously injected to the HeLa-Luc tumor model mice *via* tail vein at an RNP dose of 38.4 μg/mouse on day 0, day 2 and day 4. The tumor tissue was harvested on day 16. Tumor tissues were lysed in a lysis buffer supplemented with protease and phosphatase inhibitors, and 20 μg of protein was resolved by SDS-PAGE. Subsequently, the protein was transferred onto PVDF membranes, and the membranes were treated in the same manner as for Western blot to observe Luc expression *in vitro*. The band intensity was calculated using the Image Lab Software, and the band intensity of Luc was normalized by that of ß-actin for densitometric quantification.

2.23. Anti-tumor study. The subcutaneous HeLa-Luc tumor model or HCT116 tumor model were prepared by subcutaneously into the back of BALB/c nude mouse (4.5×10^6 cells/mouse) on day 0. Once tumors grew to approximately 30 mm^3, we intravenously injected RNP samples into the tail vein at a dose of 38.4 μg per mouse on days 11, 13, and 15.RNP was formed of Cas9 and sgRNA targeting PLK1/Luc for the treatment of HeLa-Luc tumor model mice, or $KRAS^{G13D}$for the treatment of HCT116 tumor model. The sgRNA designed to target $KRAS^{G13D}$ incorporates the G13D mutation, specifically recognizing the mutated form of the KRAS gene (Table. S1). The tumor size was measured using a caliper, and the tumor volume (V) was calculated using the following equation: $V = ab^2/2$, where a is the major axis, and b is a minor axis.

2.24. Western blot to detect PLK1 expression *in vivo*. RNP samples were intravenously injected to the HeLa-Luc tumor model mice *via* tail vein at an RNP dose of 38.4 μg/mouse on day 0, day 2 and day 4. The tumor tissue was harvested on day 5. The tumor was treated in the same manner as the protocol for detecting Luc expression *in vivo* by Western blot. The extracted protein was separated by SDS-PAGE, followed by transferring onto a PVDF membrane. The membranes were blocked using 5 % BSA in TBS-T for 1 hour and washed with TBS-T. The membranes were incubated for overnight at 4 °C with anti-PLK1 antibody (1:2000, Abcam) or ß-actin antibody (1:6000, Abcam) dissolved in the immunoreaction enhancer solution. After washing 3 times with TBS-T, HRP-conjugated anti-rabbit antibodies were incubated as secondary antibodies. Membranes were incubated with SuperSignal West Dura Extended Duration Substrate (Thermo Fisher Scientific) and visualized using a chemiluminescence imaging system. The band intensity was calculated by the Image Lab Software, and the band intensity of PLK1 was normalized by that of ß-actin for densitometric quantification.

2.25. Immunofluorescence staining. For histological analysis, harvested tumor samples from the RNP-treated groups were fixed in 4% paraformaldehyde overnight at 4 °C. The fixed tissues were equilibrated in 15% and 30% sucrose solutions for 2 h each, embedded in OCT compound, and sectioned at 5 μm. Cryosections were permeabilized with 0.2% Triton X-100 for 15 min and blocked with 2% BSA in PBS for 1 h at room temperature. The sections were then probed with primary antibodies, including rabbit anti-Luc (1:100; Abcam) and anti-PLK1 (1:100; Abcam), for 2 h at room temperature. Following three rinses with PBS-T, cells were labeled with Alexa Fluor 647-conjugated anti-rabbit IgG (1:500; Cell Signaling Technology) for 1 h at room temperature. After washing thrice with PBS-T, the specimens were mounted using Vector TrueVIEW Autofluorescence Quenching Kit with DAPI (Vector Laboratories) and visualized under a BZ-X800 fluorescence microscope (Keyence).

2.26. Toxicity study. RNP samples containing PLK1 targeting sgRNA were intravenously injected to female 7-week-old BALB/c nude mice *via* tail vein at an RNP dose of 38.4 μg/mouse on day 0, -3, and -6. Seven days post treatment, the blood was collected, and plasma was collected by centrifuging the blood (5000 rpm, 10 min). The RBC (red blood cells), WBC (white blood cells), PLT (platelet) in blood was analysed an Automatic Multiple Blood Cell Counter (POCH-100IVDIFF, Sysmex, Lincoln-shire, IL, U.K.). GOT/AST (Glutamic Oxaloacetic Transaminase/Aspartate transaminase), GPT-P (glutamic pyruvic transaminase), BUN (blood urea nitrogen), CRE (creatinine), and LDH (lactic acid dehydrogenase) levels were analysed in the plasma using FujiDri-Chem (Fujifilm, Tokyo, Japan).

2.27. Statistical analysis. Statistical significance was determined using Student's t-test for comparisons between two groups. For multiple comparisons, one-way analysis of variance (ANOVA) followed by Tukey's post-hoc test was performed.

3. Results

3.1. Preparation and characterization of RNP ternary complexes

Cas9/sgRNA RNP was prepared by mixing Cas9 protein with two nuclear localization sequences (2NLS) and sgRNA in aqueous solution. RNP was mixed with TA at various TA to RNP ratios ([TA]/[RNP]) in aqueous solution to prepare RNP/TA complexes. This [TA]/[RNP] ratio is an important indicator of complex formation because excess amounts of TA induce aggregation and precipitation of RNP owing to their hydrophobic nature [21]. Based on a previous study [19], the formation of the RNP/TA complex was evaluated by light scattering analysis whereby the formation of a large aggregate was reflected as a significant increase in the scattered light intensity (derived count rate) (Fig. S1). For [TA]/[RNP] ≤ 30, the derived count rate barely increased with the addition of TA, whereas a steep increase in the derived count rate was observed at [TA]/[RNP] ≥ 50, suggesting distinct aggregation of RNP/TA complexes at [TA]/[RNP] ≤ 50. Thus, [TA]/[RNP] was set to 30 for all subsequent measurements.

We prepared two types of PBA-conjugated polymers: P[Glu(DET)/Glu(FPBA)] and P[Lys/Lys(FPBA)], in which 14 and 10 FPBA moieties were conjugated to side chains on the poly[Glu(DET)] component of PEG-P[Glu(DET)] block copolymer and on the poly(L-Lysine) component of PEG-PLys block copolymer, respectively, *via* amide linkage (M_n of PEG:10,000, the DP of Glu(DET) and Lys: 24 and 20, respectively) (Figs. 1B, S2-S3 and Table S1). The FPBA moiety had a pK_a of 7.2, thus forming a stable boronate ester with the galloyl groups of TA at physiological pH (~ 7.4) [26]. In our previous study, P[Lys/Lys(FPBA)] was used to form protein ternary complexes with GFP/TA and b-gal/TA complexes, and the conjugation rate of FPBA to the Lys side chain was set to 50% to maintain the water solubility of the amine group residues of Lys, and the multiple FPBAs may permit the formation of multivalent boronate esters with the galloyl groups of TA [19, 25]. In addition, amine groups have been reported to improve the stability of nearby boronate esters through coordination bonding with boronic acid [27]. Thus, to confirm the effect of the amine structures in the residues, P[Glu(DET)/Glu(FPBA)] with ethylenediamine moieties was used to prepare RNP/TA/PBA-conjugated polymer ternary complexes. The synthesis of each PBA-conjugated polymer was confirmed using GPC and ^{1}H NMR spectroscopy (Figs. S4–S7).

P[Lys/Lys(FPBA)] or P[Glu(DET)/Glu(FPBA)] was mixed with the RNP/TA complex in aqueous solution, and the formation of RNP samples was evaluated by electrophoresis (Fig. 2A). To visualize the RNP samples, they were stained with CBB. Compared to RNP alone, the RNP/TA complexes exhibited longer migration toward the anode because of the anionic properties of TA, which is in good agreement with our previous studies [19, 25]. However, both RNP ternary complexes migrated to the cathode, suggesting that the RNP/TA complexes interact with PBA-conjugated polymers with cationic amine residues to form RNP ternary complexes. Interestingly, although the lanes of RNP/TA/P[Lys/Lys(FPBA)] contained only a spot, the lane of RNP/TA/P[Glu(DET)/Glu(FPBA)] contained a slight smear in addition to a spot, indicating a difference in the formation and stability of the RNP ternary complexes. Next, the hydrodynamic diameter and number of RNPs in each RNP complex were evaluated using fluorescence correlation spectroscopy (FCS) (Figs. 2B and C). Note that, this number of RNPs provides an average loading value, rather than indicating that every individual nanoparticle strictly contains one RNP molecule. The hydrodynamic diameter of RNP/TA was 48.5 nm, which is significantly larger than the RNP alone (13 nm) in aqueous solution, because a single RNP/TA complex contained ~ 3 RNP particles, indicating that the RNP/TA complex was micro-aggregated due to the hydrophobic interaction of TA (Fig. 2C). After adding polymers to the RNP/TA complexes, the association number of the RNP ternary complexes decreased to ~ 1.0, and the hydrodynamic diameters of the RNP ternary complexes with P[Glu(DET)/Glu(FPBA)] and P[Lys/Lys(FPBA)] changed to 21.7 nm and 27.9 nm, respectively, which are smaller than the RNP/TA complex but larger than single RNP. The DLS histogram revealed a single peak in all RNP samples (PDI of RNP, RNP/TA, and RNP/TA/P[Glu(DET)/Glu(FPBA)], and RNP/TA/P[Lys/Lys(FPBA)]: 0.35, 0.31, 0.29, and 0.13 respectively) (Fig. S8). Transmission electron microscopy (TEM) images showed that the RNP, RNP/TA/P[Glu(DET)/Glu(FPBA)], and RNP/TA/P[Lys/Lys(FPBA)] ternary complexes exhibited spherical and relatively dispersed morphologies, whereas RNP/TA showed micro aggregation in the dry state (Fig. S9). These results suggest that these polymers interacted with the RNP/TA complex and improved the dispersity owing to the hydrophilic

properties of the polymers, strongly indicating the formation of RNP ternary complexes. Meanwhile, the hydrodynamic diameter of RNP/TA/P[Glu(DET)/Glu(FPBA)] was slightly smaller than that of RNP/TA/P[Lys/Lys(FPBA)], suggesting a difference in the stability and number of polymers in the complex, which is consistent with the electrophoresis results. To further investigate the differences between the polymers, the apparent affinity of the polymers for gallic acid (GA), which is a component molecule of TA, was measured by Alizarin red S (ARS) (Fig. 2D) [22]. P[Lys/Lys(FPBA)] exhibited almost a 12-fold stronger apparent binding affinity for GA than P[Glu(DET)/Glu(FPBA)] because of the difference in the number of amines and the structure of the residual chain on the polymers. To summarize, both P[Glu(DET)/Glu(FPBA)] and P[Lys/Lys(FPBA)] could form RNP ternary complexes with the RNP/TA complex *via* boronate esters; however, P[Lys/Lys(FPBA)] interacted more strongly with the RNP/TA complex than P[Glu(DET)/Glu(FPBA)].

3.2. Stability of RNP ternary complexes under biological conditions

Since proteins in the blood, such as albumin, are known to interact with TA and protein/TA complexes [28], we used FCS to measure the hydrodynamic diameter of the RNP samples in the presence of FBS (Fig. 2E). The hydrodynamic diameter of the RNP was not significantly changed with increasing FBS concentrations, while the hydrodynamic diameter of the RNP/TA complex decreased from 49.0 nm to 12.2 nm when the FBS concentration was increased to 10%. It can be assumed that serum proteins in FBS interact with excess TA in the micro-aggregated RNP/TA complex and partially detach TA from the RNP/TA complex. Upon further increase of the FBS concentration to 50%, the diameter of the RNP/TA complex gradually increased to 14.0 nm, indicating that the serum components gradually interacted with RNP/TA complex. On the other hand, the hydrodynamic sizes of both RNP ternary complexes were stable even in the presence of 50% FBS. This behavior indicates that the PEG in PBA-conjugated polymers likely functioned as a shell and suppressed the interaction of the RNP/TA complex with FBS, consistent with our previous study [19]. The stability of the RNP complexes was further confirmed by electrophoresis following incubation with FBS (Fig. S10). After incubation of each RNP sample with different concentration of FBS in aqueous solution at 37°C for 24 hours, the RNP samples were electrophoresed, and the sgRNAs were stained with SYBR™ green II. In the presence of FBS, the RNP-derived band disappeared, and only the FBS-derived smear band was observed, suggesting that FBS components may degrade sgRNA. Meanwhile, both RNP ternary complexes exhibited bands of equivalent position and intensity to the untreated RNP ternary complex even in the presence of FBS. These results strongly suggest that the RNP ternary complex maintains stable particle formation and can protects the core RNP even in serum environments without apparent interference from the protein corona.

Next, we evaluated the resistance of the RNP samples to enzymatic degradation in the presence of RNase by electrophoresis (Fig. S11). RNase is present in the body and degrades sgRNAs of RNPs administered *in vivo*, resulting in decreased gene editing efficacy [29]. After incubation of each RNP sample with RNase in aqueous solution, the RNP samples were electrophoresed, and the sgRNAs were

stained with SYBR™ green II. The stained sgRNA bands of RNPs and RNP/TA complexes disappeared after RNase treatment, indicating degradation of the loaded sgRNA. In contrast, in both ternary complex lanes, the RNase-treated samples had band intensities similar to those of the untreated samples. This can be explained by the ternary complexes preventing RNase from accessing the core of the RNPs owing to the exclusion volume effect of the PEG shell. These results strongly suggest that P[Lys/Lys(FPBA)] and P[Glu(DET)/Glu(FPBA)] were sufficient to cover the RNP/TA complex.

The pH responsiveness of P[Glu(DET)/Glu(FPBA)] and P[Lys/Lys(FPBA)] was compared by measuring the hydrodynamic diameter of RNP ternary complexes in various pH solutions using FCS. The complexes exhibited a size reduction in response to decreasing pH, eventually reaching the size of RNP itself at pH 5.5 (Fig. S12). This behavior is consistent with previous studies conducted with GFP and β-gal [19, 25].

3.3. Cellular uptake and subcellular distribution

To quantify cellular uptake, the fluorescence intensity of Cas9-GFP in HeLa-Luc cells was measured using flow cytometry (FCM) (Fig. 3A). The cellular uptake of the RNP/TA complex was decreased to 40% of that of the RNPs, suggesting that serum components in the medium may detach TA from the RNP/TA complex. In addition, the serum/TA complex might compete with the RNP/TA complex for interaction with the cell membrane, which inhibited the cellular uptake of the RNP/TA complex. Both RNP/TA/P[Glu(DET)/Glu(FPBA)] and RNP/TA/P[Lys/Lys(FPBA)] ternary complexes also showed a decreased cellular uptake, but RNP/TA/P[Lys/Lys(FPBA)] ternary complexes demonstrated much lower cellular uptake, because RNP/TA/P[Lys/Lys(FPBA)] ternary complexes has more stable PEG-shell coating than RNP/TA/P[Glu(DET)/Glu(FPBA)] (Figs. 2A, and 2B), suppressing their interaction with cell membrane [30]. Although flow cytometry suggested relatively high cellular association of naked RNPs, it should be noted that flow cytometry quantifies total cellular fluorescence and does not distinguish between membrane-bound and internalized materials. Therefore, biomolecules that strongly adsorb to the cell membrane can produce high fluorescence signals without efficient intracellular delivery. To clarify this point, the intracellular localization of each sample was further examined by confocal laser scanning microscopy.

The subcellular distribution of each RNP sample was observed in HeLa–Luc cells using Confocal Laser Scanning Microscopy (CLSM) 24 hours after sample treatment, and endo/lysosomes and nuclei were stained with LysoTracker™ Red DND-99 (red) and Hoechst 33342 (Blue), respectively (Fig. 3B, Fig. S13). CLSM observations revealed that the RNPs and RNP/TA complexes (green) were localized with the cell membrane, similar to a previous study [31]. In contrast, the green fluorescence of both RNP ternary complexes not only overlapped with the red fluorescence (LysoTracker) and turn to yellow, but also diffused throughout the cells and overlapped with the blue (nucleus) fluorescence. This indicates that the polymer coating facilitated the endocytosis-mediated internalization of the RNP complexes, followed by their escape into the cytosol and subsequent translocation to the nucleus. Furthermore, the subcellular distribution images of RNP ternary complexes containing Cas9-GFP (green) and Alexa647-labelled PBA-conjugated polymers (orange) indicated that the intracellular distribution behavior of RNP

and PBA-conjugated polymer did not correlate, and the Pearson correlation coefficient for both ternary complexes was approximately 0.1 (Fig. S14). Generally, the Pearson correlation coefficient below 0.2 indicates no association between the behavior of the two fluorophores, suggesting that RNP has dissociated from PBA-conjugated polymers within cells.

3.4. *In vitro* gene knockout study

To evaluate the gene knockout efficiency of the RNP ternary complexes, we incubated HeLa–Luc cells with RNP samples containing luciferase (Luc)-targeted sgRNA (Table. S2). The sgRNA sequence exhibited Luc gene editing in the previous study [14]. After 72 hours of incubation, the luminescence intensity of treated cells was measured using a luminometer. (Fig. 4). According to the Cell counting kit-8 (CCK-8) assay, RNP/TA/P[Lys/Lys(FPBA)] ternary complexes showed slight toxicity compared to RNP/TA/P[Glu(DET)/Glu(FPBA)]. This might be because the primary amine structure in P[Lys/Lys(FPBA)] disrupted the cell membrane. To see the gene knockout efficiency, the luminescence intensity was normalized to the cell's viability. The cells treated with RNP, or the RNP/TA complex exhibited similar luminescence intensity as D-PBS(-)-treated cells, indicating that RNP alone and the RNP/TA complex did not achieve adequate gene knockout in HeLa–Luc cells because of localization on the cell membrane and low nuclear transition. By contrast, RNP/TA/P[Glu(DET)/Glu(FPBA)] and RNP/TA/P[Lys/Lys(FPBA)] ternary complexes showed 13% and 40% decreases, respectively, in the luminescence intensities of the treated cells, indicating that the coating of the RNP/TA complexes with PBA-conjugated polymers augmented the gene knockout efficiency because of the enhanced intracellular uptake and nuclear translocation. The reduction of Luc expression was further confirmed by Western blot (Fig. S15). Compared to PBS-treated group, the signal was weaker in RNP/ProDeliverIN-treated cells and both RNP ternary complexes-treated cells, which is consistent with the result of Luc activity assay (Fig. 4A). The RNP/TA/P[Lys/Lys(FPBA)] ternary complex exhibited high gene knockout efficiency in Fig. 4A despite similar intracellular uptake of RNP/TA/P[Glu(DET)/Glu(FPBA)]. This may be because the RNP/TA/P[Lys/Lys(FPBA)] complex was covered by more polymer chains than the RNP/TA/P[Glu(DET)/Glu(FPBA)] complex owing to its high stability. Hence, a large number of P[Lys/Lys(FPBA)] chains may affect the endosomal membrane, resulting in high gene editing efficiency.

Knockout of Luc gene was further confirmed by T7 Endonuclease I (T7EI) assay (Fig. 4C). T7EI assay demonstrated that target DNA bands (820 bp) were cut into two cleavage bands (740 bp and 80 bp) at the ternary complex treated group, and no cleavage bands were observed with D-PBS(-)-treated group. In addition, to evaluate *in vitro* gene editing ability of RNP ternary complexes, we mixed RNP samples with an extracted and amplified Luc target DNA at physiological pH (~ 7.4) or endosomal acidic pH (~ 5.5), and the cleaved DNA was analyzed by gel electrophoresis. (Fig. S16). The DNA cleavage capacity of an RNP alone was equivalent at pH 5.5 and pH 7.4. Meanwhile, both RNP ternary complexes showed a single band derived from substrate DNA at pH 7.4, but showed 3 different bands derived from DNA cleaved into longer and shorter fragments at pH 5.5, indicating that RNP ternary complexes can release the loaded RNP in response to the endosomal acidic pH and recover the gene knockout function within the cells.

3.5. Biodistribution of the RNP ternary complexes

To examine the biodistribution profile of the RNP ternary complexes, we intravenously injected Cy5-labeled sgRNA alone and each RNP sample, (Cas9: 32.0 μg/mouse, sgRNA: 6.4 μg/mouse), into BALB/c nude mice bearing HeLa-Luc tumors, and the amounts of Cy5-labeled sgRNA in the tumors and normal organs were quantified using fluorophotometer (Fig. 5). The blood retention levels of RNP were 6.5% and 0.4% ID/mL plasma at 1 and 2 h after intravenous injection, respectively, whereas those of sgRNA alone were only 2.8% and 0.1% ID/mL plasma at 1 and 2 h, respectively (Fig. 5A). In addition, accumulation of the sgRNA alone in liver (0.8% ID/g liver) and kidney (1.3% ID/g kidney) at 2 h was lower than that of the RNP (6.0% ID/g liver and 6.0% ID/g kidney) (Figs. 5C and 5G). These differences indicate that stable RNP complexes formed even *in vivo*. The RNP/TA complexes had values of 2.5% and 0.7% ID/mL in plasma after 1 and 2 h, respectively, indicating a similar blood retention profile to RNP alone (Fig. 5A). However, the RNP alone exhibited considerable accumulation in liver and kidney (12.7% and 7.8% ID/g organ, respectively), whereas the RNP/TA complex exhibited high accumulation in liver and spleen (9.5% and 14.3% ID/g organ, respectively), with only 0.67% ID/g organ in kidney, likely owing to the TA-coating effect [25] (Figs. 5C and 5D). On the other hand, both RNP ternary complexes exhibited prolonged blood retention compared to the RNP alone and the RNP/TA complex. The blood retention values of the RNP/TA/P[Glu(DET)/Glu(FPBA)] ternary complexes were 29.9, 21.3, and 12.2% ID/mL plasma at 1, 2, and 6 h, respectively, and those of the RNP/TA/P[Lys/Lys(FPBA)] were 15.9, 10.1, and 5.6% ID/mL plasma at 1, 2, and 6 h, respectively (Fig. 5A). Such prolonged blood retention was probably due to the PEG shell, which prevented interaction with blood components, and the substantial coverage of RNP/TA by both polymers. Incidentally, that of the RNP/TA/P[Glu(DET)/Glu(FPBA)] ternary complex was approximately twice that of the RNP/TA/P[Lys/Lys(FPBA)] ternary complex. The organ accumulation profiles were also different, with the RNP/TA/P[Glu(DET)/Glu(FPBA)] ternary complex exhibiting high accumulation in kidney (46.6% ID/g kidney at 2 h), whereas the RNP/TA/P[Lys/Lys(FPBA)] ternary complex exhibited low accumulation in kidney (4.5% ID/g kidney at 2 h) (Figs. 5E and 5F). As an alternative to accumulation in kidney, the RNP/TA/P[Lys/Lys(FPBA)] ternary complex mainly accumulated in liver (36.6% ID/g liver at 2 h). This difference may be explained by differences in the structural stability of the ternary complexes (Figs. 5E and 5F). As shown in Fig. 2D, P[Lys/Lys(FPBA)] exhibited a stronger apparent affinity for GA than P[Glu(DET)/Glu(FPBA)], suggesting that the RNP/TA/P[Lys/Lys(FPBA)] ternary complex may be tightly covered by more polymer chains and exhibit more structural stability than the RNP/TA/P[Glu(DET)/Glu(FPBA)] ternary complex. The zeta-potential values of both TA/PBA-conjugated polymers were comparable, and the difference in the density of PBA-conjugated polymers in the ternary complexes may cause accumulation in the liver (Fig. S17). Note that, both RNP ternary complexes exhibited comparably low accumulation in spleen (≤ 10% ID/g spleen).

Regarding tumor accumulation, the RNP and RNP/TA complex exhibited accumulation of approximately 1.0% ID/g tumor. On the other hand, both RNP ternary complexes exhibited 2%–4% ID/g tumor accumulation, achieving higher tumor accumulations than RNP and RNP/TA (Fig. 5B). These tumor accumulation properties are consistent with those of our previous studies [19, 25]. This significantly

enhanced tumor accumulation may be due to an enhanced permeability and retention (EPR) effect of the ternary complex.

3.6. *In vivo* gene knockout study

To evaluate the *in vivo* gene editing efficiency, we intravenously injected each RNP sample (Cas9: 32.0 μg/mouse, sgRNA: 6.4 μg/mouse) containing Luc-targeted sgRNA into BALB/c nude mice bearing HeLa-Luc tumors. The luminescence intensities of the tumors were measured semi-quantitatively using an *in vivo* imaging system (IVIS) before sample injections and 3 and 7 days after sample injections (Figs. 6A and B). The luminescence intensity of each mouse on day 0 was set to 1 to calculate the time-dependent changes in the luminescence intensities (Fig. 6C). Note that the injection of RNP samples had no effect on tumor size growth (Fig. S18). The luminescence intensities at the tumor sites of RNP-and RNP/TA-treated mice were slightly lower than those of D-PBS(-)-treated mice at both 3 and 7 days, indicating the *in vivo* gene knockout efficiency of RNP. However, both RNP ternary complexes significantly suppressed the luminescence intensities of the tumors compared with other RNP samples on days 3 and 7, which can be attributed to high tumor accumulation. The luminescence intensities at the tumor sites of mice treated with the RNP ternary complexes on day 7 decreased compared to those on day 3, which suggests that the polymer coated RNP ternary complex was gradually translocated to the cell nucleus, possibly because of the modulated cellular uptake and transition to the cytoplasm.

For a more quantitative evaluation, tumors were collected and homogenized on day 7, and the luminescence intensity of the tumors was measured by Luc assay (Fig. 6D). The RNP and RNP/TA exhibited a slight decrease in the luminescence intensities of the homogenized tumors to 96% and 74%, respectively, compared to the treatment with D-PBS(-), and the tendency was similar with the luminescence intensity from IVIS. Similar to the trend in luminescence intensity with IVIS, the RNP/TA/P[Glu(DET)/Glu(FPBA)] and RNP/TA/P[Lys/Lys(FPBA)] ternary complexes have exhibited clear gene editing effects and significantly decreased the luminescence intensities of the tumors to 54% and 36%, respectively, compared to that of D-PBS(-). In the luminescence measurement, the *in vivo* gene-editing effect of the RNP/TA/P[Lys/Lys(FPBA)] ternary complex was higher than that of the RNP/TA/P[Glu(DET)/Glu(FPBA)] ternary complex, although the tumor accumulation was comparable. The difference in gene editing effects can be explained by the higher *in vitro* gene knockout efficiency of RNP/TA/P[Lys/Lys(FPBA)] (Fig. 4A), which suggests that the RNP/TA/P[Lys/Lys(FPBA)] ternary complex is more effective as a systemically administered RNP delivery system against tumors. To analyze the Luc expression level in the tumors, RNP samples were administrated intravenously 3 times into HeLa-Luc tumor model mice. At 12 days post RNP samples injection, the tumors were analyzed by Western blot and were fixed with paraformaldehyde (PFA) for immunofluorescence staining. (Fig. 6E, 6F, S16). The Western blot image demonstrated that RNP treatment alone slightly reduced the Luc expression compared with non-treatment, while treatment with both RNP ternary complexes significantly reduced the Luc expression even compared to the RNP-treated group. This reduction in the Luc expression was further verified by immunofluorescence staining (Fig. S19), confirming decreased red Luc signal in the ternary complex-treated groups compared with non-treatment and RNP treatment groups. In addition,

using the extracted and amplified target Luc DNA region, TIDE (Tracking of Indels by Decomposition) analysis was carried out to determine the indel frequency in the tumor samples (Fig. 6G). While RNP alone did not exhibit apparent indel frequency with only 1.5%, RNP/TA/P[Lys/Lys(FPBA)] showed 37.2% of the indel frequency (Fig. S20). RNP/TA/P[Glu(DET)/Glu(FPBA)] demonstrated the similar indel frequency with RNP/TA/P[Lys/Lys(FPBA)] (date not shown). Even there was no difference in the tumor volume (Fig. S21), RNP ternary complexes showed gene editing in the tumor sites. The Indel frequency was comparable in these ternary complexes, which is consistent with the luminescence measurement in Fig. 6D.

3.7. Anti-tumor study

The therapeutic effect of RNP ternary complexes was examined using BALB/c nude mice bearing HeLa-Luc tumors (Figs. 7A). We intravenously injected RNP samples (Cas9: 32.0 μg/mouse, sgRNA: 6.4 μg/mouse) containing polo like kinase 1 (PLK1) gene-targeted sgRNA 3 times, every other day (Table. S2). Naked RNP and RNP/TA complex did not show tumor growth inhibition effects due to the low accumulation and gene knockout efficacy in tumor sites. Similarly, RNP/TA/P[Lys/Lys(FPBA)] ternary complexes containing Luc gene-targeted sgRNA did not show tumor growth suppression (Fig. S21). Meanwhile, both RNP ternary complexes achieved the significant inhibition of the tumor growth as a result of the efficient *in vivo* tumor gene editing. Western blot and immunofluorescence staining further demonstrated the PLK1 knockout within the tumors (Fig. S22). According to the Western blot image, RNP/TA/P[Glu(DET)/Glu(FPBA)] therapy significantly reduced the PLK1 expression level, and RNP/TA/P[Lys/Lys(FPBA)] therapy also showed a tendency to decrease PLK1 expression compared to non-treated group and RNP treated group (Fig. S22A and B). Similarly, immunofluorescence staining observations revealed that both ternary complexes reduced the red PLK1 signal compared to PBS and RNP treated group (Fig. S22C), indicating *in vivo* PLK1 knockout function of RNP ternary complexes. TIDE analysis showed that ~ 2% of Indels were introduced in the RNP ternary complexes (Fig. S23). In addition, treatment of the RNP ternary complexes exhibited similar weight changes and blood parameter values with treatment of D-PBS(-), indicating negligible adverse effects. (Figs. 7B and S24, respectively).

We then evaluated targeted gene editing efficacy using tumor cell line with a mutation in cancer related gene (Figs. 7C and D). The mutation in Kirsten rat sarcoma virus (KRAS) promote malignancy of the cells, which is an undruggable target other than gene knockout technology. Especially, Human Colon Cancer (HCT) 116 cell line has a G13D mutation in KRAS gene [32]. Using HCT 116 tumor bearing model mice, we also examined anti-tumor effect of RNP ternary complexes containing mutated KRAS-targeted sgRNA in the similar manner with the PLK1 study. The administration of RNP/TA/P[Lys/Lys(FPBA)] ternary complexes significantly impeded tumor growth compared to D-PBS(-) and RNP treatments, indicating the efficacy of this delivery system for precise gene editing in targeted cells, thus highlighting its therapeutic potential.

4. Discussion

The CRISPR/Cas system, derived from the bacterial immune system, has garnered significant attention as a transformative gene-editing tool. Gene-editing therapies hold tremendous promise for addressing various genetic disorders. To date, CRISPR/Cas-based therapies have been applied in clinical trials for congenital diseases, including Hemophilia and Mucopolysaccharidosis, typically *via* local injection. However, systemic application remains challenging due to limitations in site-specific targeting, insufficient stability in the bloodstream, and risks of off-target effects, thereby impeding clinical translation. While lipid-based nanoparticles have been primarily used for systemic genome editing strategies, their application has been limited mainly to the liver and spleen with a reticuloendothelial system[14, 33, 34]. There have been few reports of their use in other organs, such as tumors. In this study, we engineered a systemically applicable RNP delivery system utilizing PBA-conjugated polymers and tannic acid for tumor gene editing therapy. Most previous studies utilizing TA–PBA interactions in biomaterial-based drug delivery systems have primarily focused on the construction of pH-responsive hydrogels or applications involving local administration[35, 36]. In contrast, the present study demonstrates the direct encapsulation of a large protein-nucleic acid complex within a well-defined supramolecular nanoscale assembly, enabling stimulus-responsive intracellular release and systemic *in vivo* tumor genome editing within a single polymer platform.

This ternary complex demonstrated exceptional tumor accumulation and effective gene-editing capabilities, showcasing its potential for cancer therapy. The RNP ternary complex is shielded by a PEG layer, which mitigates interactions with blood components and enhances circulatory stability. Its relatively large particle size compared to RNP, optimized for encapsulating a single RNP within the core, facilitates passive accumulation in tumor tissue via the enhanced permeability and retention (EPR) effect. In this biodistribution study, we observed that altering the side chains of the PBA-conjugated polymer influenced the biodistribution of the complex, suggesting the potential for organ-specific delivery. For instance, the P[Lys/Lys(FPBA)] polymer having primary amine side chain exhibited increased accumulation in the liver, whereas the P[Glu(DET)/Glu(FPBA)] polymer having ethylenediamine side chain predominantly localized in the kidney.

These findings highlight the importance of polymer structural modifications in modulating delivery profiles to minimize off-target effects and exhibit efficient gene editing in various tissues for treatment of genetic diseases. Our results demonstrated robust tumor-specific gene editing and significant tumor growth suppression without systemic toxicity. In the PLK1 and mutated KRAS editing study, the tumor growth was delayed even the knockout efficiency was a few percent. Still the kinetics of the editing efficiency in the tumor are under investigation, editing oncogene has a potential to treat the cancer. However, while tumor growth was arrested, complete remission was not observed in both anti-tumor study, indicating the inherent challenges of gene-editing-based cancer therapies. To further optimize efficacy, future efforts should focus on enhancing tumor accumulation and retention of the RNP complex. For example, modifying the PBA-conjugated polymer with tumor-targeting ligands, such as cyclic RGD peptides or glucose, could improve tumor specificity and accumulation[37]. Additionally, combining gene-editing therapies with other therapeutic modalities such as Olaparib, which is a type of PARP inhibitor against ovarian cancer, could yield synergistic effects[38]. In conclusion, our ternary

complex system represents a promising strategy for tumor-specific gene delivery and editing, with significant potential to enhance current cancer therapies. By enabling the precise and effective delivery of active RNPs, this approach paves the way for a rational and integrative design of cancer treatment strategies.

5. Conclusion

In this study, we constructed systemic applicable RNP delivery systems by sequential self-assembly utilizing TA and PBA-conjugated polymers. This sequential self-assembled nanocarrier enhanced the tumor accumulation of RNP and demonstrated significant *in vivo* gene editing. In addition, RNP ternary complex armored with cancer gene targeting sgRNA introduced suppressed tumor growth in different tumor models. This RNP delivery system will offer as a systemic applicable cancer gene therapy.

Abbreviations

CRISPR, Clustered regularly interspaced short palindromic repeats; Cas9, CRISPR-associated protein 9; sgRNA, single guide RNA, RNP, ribonucleoprotein. TA, tannic acid; PBA, phenylboronic acid; PEG, poly(ethylene glycol); PEG-PBLG, PEG–*b*-poly(γ-benzyl-L-glutamate); PEG-PLys, PEG-*b*-poly(l-lysine); DET, diethylenetriamine; FPBA, 4-carboxy-3-fluorophenylboronic acid; PBA, Phenylboronic acid; KRAS, Kirsten rat sarcoma virus; PLK1, polo-like kinase 1; DLS, dynamic light scattering; FCS, fluorescence correlation spectroscopy; ARS, Alizarin red S; MES, 2-Morpholinoethanesulfonate; GFP, green fluorescent protein; CLSM, Confocal Laser Scanning Microscopy; T7EI, T7 Endonuclease I; Luc, luciferase; IVIS, *in vivo* imaging system; TIDE, Tracking of Indels by Decomposition; TBS-T, Tris-Buffered saline with Tween 20; HRP, Horseradish peroxidase; PVDF, Polyvinylidene difluoride; SDS-PAGE, Sodium dodecyl sulfate–polyacrylamide gel electrophoresis; BSA, bovine serum albumin; PFA, Paraformaldehyde; PDI, Protein disulfide isomerase; TEM, Transmission electron microscopy.

Declarations

Ethics approval and consent to participate

Not applicable.

Consent for publication

Not applicable.

Availability of data and materials

The datasets used and/or analysed during the current study are available from the corresponding author on reasonable request.

Competing interests

Y.H., T.N., and N.N. are inventors of the filed patent in Japan (2019-100395). The authors declare no competing financial interest.

Funding

This research was supported financially by the open innovation platform for industry-academia cocreation (COI-NEXT) Program (JPMJPF2202) from Japan Science and Technology Agency (JST), the Science and Technology Platform Program for Advanced Biological Medicine (JP22am0401018), and Research on Development of New Drugs (23ak0101173) from Japan Agency for Medical Research and Development (AMED), and JSPS KAKENHI (22H00581, 22K18193, 21K20513, 23H04060, 24K03278), Tokyo Institute of Technology Fund (Interdisciplinary Research Support for Scientists), Five-star Alliance from the Ministry of Education, Culture, Sports, Science, and Technology (MEXT) and the Cooperative Research Program of Network Joint Research Centre for Materials and Devices under the Grant Number 20243017 (T.N.)

Author's contribution

T.M. and Y.H. designed and performed all experiments. T.M. and Y.H. wrote the manuscript. T.C. assisted *in vivo* experiments. T.N. and Y.O. advised *in vitro* and *in vivo* experiments and proofread the manuscript. Y.M. advised polymerization. N.N. and Y.H. supervised the whole project and conceived the concept of this study. This manuscript was written through contributions of all authors. All authors have given approval to the final version of the manuscript.

Corresponding Author

* (Y.H.) honda.y.aj@m.titech.ac.jp

(N.N.) nishiyama.n.ad@m.titech.ac.jp

Acknowledgments

We thank the Division of Materials Analysis Suzukake-dai, Technical Department, Institute of Science Tokyo, for ^{1}H NMR analysis. We would like to thank Editage (www.editage.com) for English language editing.

References

1. Karimian A, Azizian K, Parsian H, Rafieian S, Shafiei-Irannejad V, Kheyrollah M, Yousefi M, Majidinia M, Yousefi B. CRISPR/Cas9 technology as a potent molecular tool for gene therapy. J Cell Physiol. 2019;234:12267–77. https://doi.org/10.1002/jcp.27972.
2. Xiao-Jie L, Hui-Ying X, Zun-Ping K, Jin-Lian C, Li-Juan J. CRISPR-Cas9: a new and promising player in gene therapy. J Med Genet. 2015;52:289–96. https://doi.org/10.1136/jmedgenet-2014-102968.

3. Barrangou R, Doudna JA. Applications of CRISPR technologies in research and beyond. Nat Biotechnol. 2016;34:933–41. https://doi.org/10.1038/nbt.3659.
4. Zhang S, Shen J, Li D, Cheng Y. Strategies in the delivery of Cas9 ribonucleoprotein for CRISPR/Cas9 genome editing. Theranostics. 2021;11:614–48. https://doi.org/10.7150/thno.47007.
5. Yue J-J, Yuan J-L, Wu F-H, Yuan Y-H, Cheng Q-W, Hsu C-T, Lin C-S. Protoplasts: From Isolation to CRISPR/Cas Genome Editing Application, Front. Genome Ed. 3 (2021) 717017. https://doi.org/10.3389/fgeed.2021.717017
6. Eoh J, Gu L. Biomaterials as vectors for the delivery of CRISPR–Cas9. Biomater Sci. 2019;7:1240–61. https://doi.org/10.1039/C8BM01310A.
7. Lino CA, Harper JC, Carney JP, Timlin JA. Delivering CRISPR: a review of the challenges and approaches. Drug Delivery. 2018;25:1234–57. https://doi.org/10.1080/10717544.2018.1474964.
8. Noroozi Z, Shamsara M, Valipour E, Esfandyari S, Ehghaghi A, Monfaredan A, Azizi Z, Motevaseli E, Modarressi MH. Antiproliferative effects of AAV-delivered CRISPR/Cas9-based degradation of the HPV18-E6 gene in HeLa cells. Sci Rep. 2022;12:2224. https://doi.org/10.1038/s41598-022-06025-w.
9. Das S, Bano S, Kapse P, Kundu GC. CRISPR based therapeutics: a new paradigm in cancer precision medicine. Mol Cancer. 2022;21:85. https://doi.org/10.1186/s12943-022-01552-6.
10. Cho EY, Ryu J-Y, Lee HAR, Hong SH, Park HS, Hong KS, Park S-G, Kim HP, Yoon T-J. Lecithin nano-liposomal particle as a CRISPR/Cas9 complex delivery system for treating type 2 diabetes. J Nanobiotechnol. 2019;17:19. https://doi.org/10.1186/s12951-019-0452-8.
11. Min Y-L, Bassel-Duby R, Olson EN. CRISPR Correction of Duchenne Muscular Dystrophy. Annu Rev Med. 2019;70:239–55. https://doi.org/10.1146/annurev-med-081117-010451.
12. Zuris JA, Thompson DB, Shu Y, Guilinger JP, Bessen JL, Hu JH, Maeder ML, Joung JK, Chen Z-Y, Liu DR. Cationic lipid-mediated delivery of proteins enables efficient protein-based genome editing in vitro and in vivo. Nat Biotechnol. 2015;33:73–80. https://doi.org/10.1038/nbt.3081.
13. Wang M, Zuris JA, Meng F, Rees H, Sun S, Deng P, Han Y, Gao X, Pouli D, Wu Q, Georgakoudi I, Liu DR, Xu Q. Efficient delivery of genome-editing proteins using bioreducible lipid nanoparticles, Proc. Natl. Acad. Sci. U.S.A. 113 (2016) 2868–2873. https://doi.org/10.1073/pnas.1520244113
14. Wei T, Cheng Q, Min Y-L, Olson EN, Siegwart DJ. Systemic nanoparticle delivery of CRISPR-Cas9 ribonucleoproteins for effective tissue specific genome editing. Nat Commun. 2020;11:3232. https://doi.org/10.1038/s41467-020-17029-3.
15. Lee K, Conboy M, Park HM, Jiang F, Kim HJ, Dewitt MA, Mackley VA, Chang K, Rao A, Skinner C, Shobha T, Mehdipour M, Liu H, Huang W, Lan F, Bray NL, Li S, Corn JE, Kataoka K, Doudna JA, Conboy I, Murthy N. Nanoparticle delivery of Cas9 ribonucleoprotein and donor DNA in vivo induces homology-directed DNA repair. Nat Biomed Eng. 2017;1:889–901. https://doi.org/10.1038/s41551-017-0137-2.
16. Mout R, Ray M, Yesilbag Tonga G, Lee Y-W, Tay T, Sasaki K, Rotello VM. Direct Cytosolic Delivery of CRISPR/Cas9-Ribonucleoprotein for Efficient Gene Editing. ACS Nano. 2017;11:2452–8. https://doi.org/10.1021/acsnano.6b07600.

17. Wang P, Zhang L, Xie Y, Wang N, Tang R, Zheng W, Jiang X. Genome Editing for Cancer Therapy: Delivery of Cas9 Protein/sgRNA Plasmid via a Gold Nanocluster/Lipid Core-Shell Nanocarrier. Adv Sci. 2017;4:1700175. https://doi.org/10.1002/advs.201700175.
18. Wan T, Pan Q, Liu C, Guo J, Li B, Yan X, Cheng Y, Ping Y. A Duplex CRISPR-Cas9 Ribonucleoprotein Nanomedicine for Colorectal Cancer Gene Therapy. Nano Lett. 2021;21:9761–71. https://doi.org/10.1021/acs.nanolett.1c03708.
19. Honda Y, Nomoto T, Matsui M, Takemoto H, Kaihara Y, Miura Y, Nishiyama N. Sequential Self-Assembly Using Tannic Acid and Phenylboronic Acid-Modified Copolymers for Potential Protein Delivery, Biomacromolecules 21 (2020) 3826–3835. https://doi.org/10.1021/acs.biomac.0c00903
20. Guo J, Suma T, Richardson JJ, Ejima H. Modular Assembly of Biomaterials Using Polyphenols as Building Blocks, ACS Biomater. Sci Eng. 2019;5:5578–96. https://doi.org/10.1021/acsbiomaterials.8b01507.
21. Shin M, Lee H-A, Lee M, Shin Y, Song J-J, Kang S-W, Nam D-H, Jeon EJ, Cho M, Do M, Park S, Lee MS, Jang J-H, Cho S-W, Kim K-S, Lee H. Targeting protein and peptide therapeutics to the heart via tannic acid modification. Nat Biomed Eng. 2018;2:304–17. https://doi.org/10.1038/s41551-018-0227-9.
22. Springsteen G, Wang B. A detailed examination of boronic acid–diol complexation. Tetrahedron. 2002;58:5291–300. https://doi.org/10.1016/S0040-4020(02)00489-1.
23. Narkar AR, Barker B, Clisch M, Jiang J, Lee BP. pH Responsive and Oxidation Resistant Wet Adhesive based on Reversible Catechol–Boronate Complexation. Chem Mater. 2016;28:5432–9. https://doi.org/10.1021/acs.chemmater.6b01851.
24. Honda Y, Nagao S, Kinoh H, Liu X, Matsudaira N, Dirisala A, Nitta-Matsutomo S, Nomoto T, Hayashita-Kinoh H, Miura Y, Okada T, Nishiyama N. Adeno-Associated Virus Self-Assembled with Tannic Acid and Phenylboronic Acid-Polymers to Evade Neutralizing Antibodies and Reduces Adverse Events, ACS Nano (2025).
25. Honda Y, Nomoto T, Matsui M, Takemoto H, Miura Y, Nishiyama N. Sequentially Self-Assembled Nanoreactor Comprising Tannic Acid and Phenylboronic Acid-Conjugated Polymers Inducing Tumor-Selective Enzymatic Activity. ACS Appl Mater Interfaces. 2021;13:54850–9. https://doi.org/10.1021/acsami.1c20188.
26. Naito M, Yoshinaga N, Ishii T, Matsumoto A, Miyahara Y, Miyata K, Kataoka K. Enhanced Intracellular Delivery of siRNA by Controlling ATP-Responsivity of Phenylboronic Acid-Functionalized Polyion Complex Micelles. Macromol Biosci. 2018;18:1700357. https://doi.org/10.1002/mabi.201700357.
27. Sun X, Chapin BM, Metola P, Collins B, Wang B, James TD, Anslyn EV. The mechanisms of boronate ester formation and fluorescent turn-on in ortho-aminomethylphenylboronic acids. Nat Chem. 2019;11:768–78. https://doi.org/10.1038/s41557-019-0314-x.
28. Xie L, Wehling RL, Ciftci O, Zhang Y. Formation of complexes between tannic acid with bovine serum albumin, egg ovalbumin and bovine beta-lactoglobulin. Food Res Int. 2017;102:195–202. https://doi.org/10.1016/j.foodres.2017.10.007.

29. Allen D, Rosenberg M, Hendel A. Using Synthetically Engineered Guide RNAs to Enhance CRISPR Genome Editing Systems in Mammalian Cells, Front. Genome Ed. 2021;2:617910. https://doi.org/10.3389/fgeed.2020.617910.
30. Hatakeyama H, Akita H, Harashima H. A multifunctional envelope type nano device (MEND) for gene delivery to tumours based on the EPR effect: A strategy for overcoming the PEG dilemma. Adv Drug Deliv Rev. 2011;63:152–60. https://doi.org/10.1016/j.addr.2010.09.001.
31. Ban Q, Yang P, Chou S, Qiao L, Xia H, Xue J, Wang F, Xu X, Sun N, Zhang RY, Zhang C, Lee A, Liu W, Lin T, Ko Y, Antovski P, Zhang X, Chiou S, Lee C, Hui W, Liu D, Jonas SJ, Weiss PS, Tseng H. Supramolecular Nanosubstrate-Mediated Delivery for CRISPR/Cas9 Gene Disruption and Deletion. Small. 2021;17:2100546. https://doi.org/10.1002/smll.202100546.
32. Alves S, Castro L, Fernandes MS, Francisco R, Castro P, Priault M, Chaves SR, Moyer MP, Oliveira C, Seruca R, Côrte-Real M, Sousa MJ, Preto A. Colorectal cancer-related mutant *KRAS* alleles function as positive regulators of autophagy. Oncotarget. 2015;6:30787–802. https://doi.org/10.18632/oncotarget.5021.
33. Kim M, Song ES, Chen JC, Chatterjee S, Sun Y, Lee SM, Wu S, Patel P, Tian Z, Kantor A, Wustman BA, Lockhart DJ, Siegwart DJ. Dual SORT LNPs for multi-organ base editing. Nat Biotechnol. 2025. https://doi.org/10.1038/s41587-025-02675-z.
34. Chen K, Han H, Zhao S, Xu B, Yin B, Lawanprasert A, Trinidad M, Burgstone BW, Murthy N, Doudna JA. Lung and liver editing by lipid nanoparticle delivery of a stable CRISPR–Cas9 ribonucleoprotein. Nat Biotechnol. 2025;43:1445–57. https://doi.org/10.1038/s41587-024-02437-3.
35. Li N, Cao Y, Liu J, Zou W, Chen M, Cao H, Deng S, Liang J, Yuan T, Wang Q, Fan Y, Zhang X. Microenvironment-responsive release of Mg^{2+} from tannic acid decorated and multilevel crosslinked hydrogels accelerates infected wound healing. J Mater Chem B. 2024;12:6856–73. https://doi.org/10.1039/D4TB01000K.
36. Liu Y, Liu K, Yan Y, Zhang X, Xiao C, Song Z, Liu B. Microenvironment-modulating hyaluronic acid-tannic acid hydrogel for peripheral nerve injury repair. Acta Biomater. 2025;207:233–47. https://doi.org/10.1016/j.actbio.2025.09.056.
37. Matsudaira N, Honda Y, Kinoh H, Liu X, Nagao S, Matsutomo-Nitta S, Haochen G, Hayashita-Kinoh H, Aizawa M, Muguruma K, Miura Y, Shishido A, Okada T, Nishiyama N. Tumor-targeted adeno associated virus-loaded complexes comprising tannic acid and phenylboronic acid-polymers for orthotopic glioblastoma therapy. J Controlled Release. 2026;389:114477. https://doi.org/10.1016/j.jconrel.2025.114477.
38. Beha MJ, Kim J, Im SH, Kim Y, Yang S, Lee J, Nam YR, Lee H, Park H, Chung HJ. Bioorthogonal CRISPR/Cas9-Drug Conjugate: A Combinatorial Nanomedicine Platform. Adv Sci. 2023;10:2302253. https://doi.org/10.1002/advs.202302253.

Figures

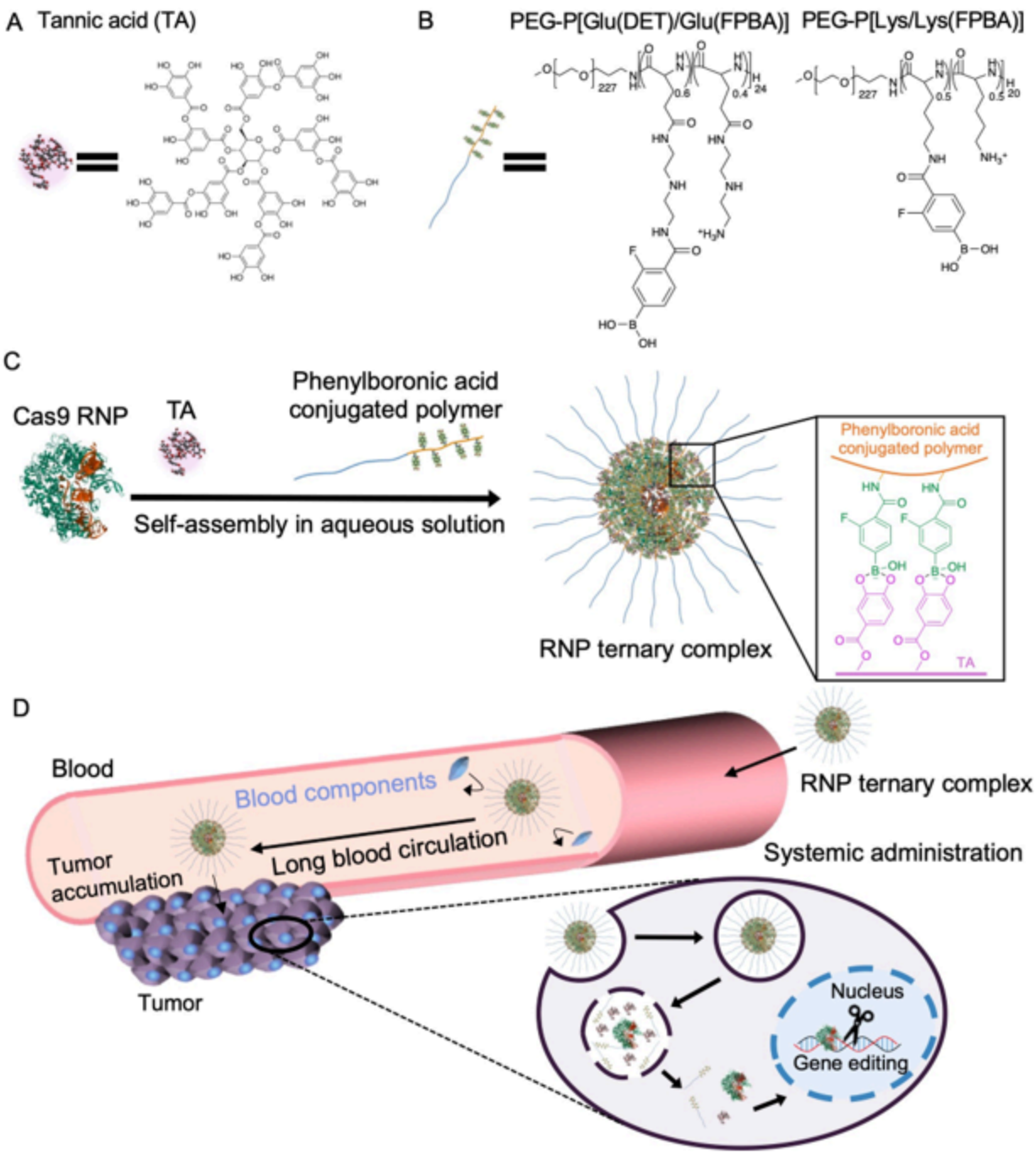

Figure 1

Schematic overview of this study. Chemical structure of (A) TA and (B) PBA-conjugated polymer. (C) Schematic procedure for preparing the ternary complex. The ternary complex is prepared through the sequential assembly of RNP, TA and PBA-conjugated polymers in an aqueous solution. (D) Illustration of the RNP ternary complex and its potential function. The ternary complex suppresses the non-specific interaction with blood components, which facilitates extended blood circulation and enhanced accumulation in tumor without compromising gene editing. After endocytic internalization, the ternary complex responds to the acidic endosomal pH to release the RNP, leading to successful tumor gene editing.

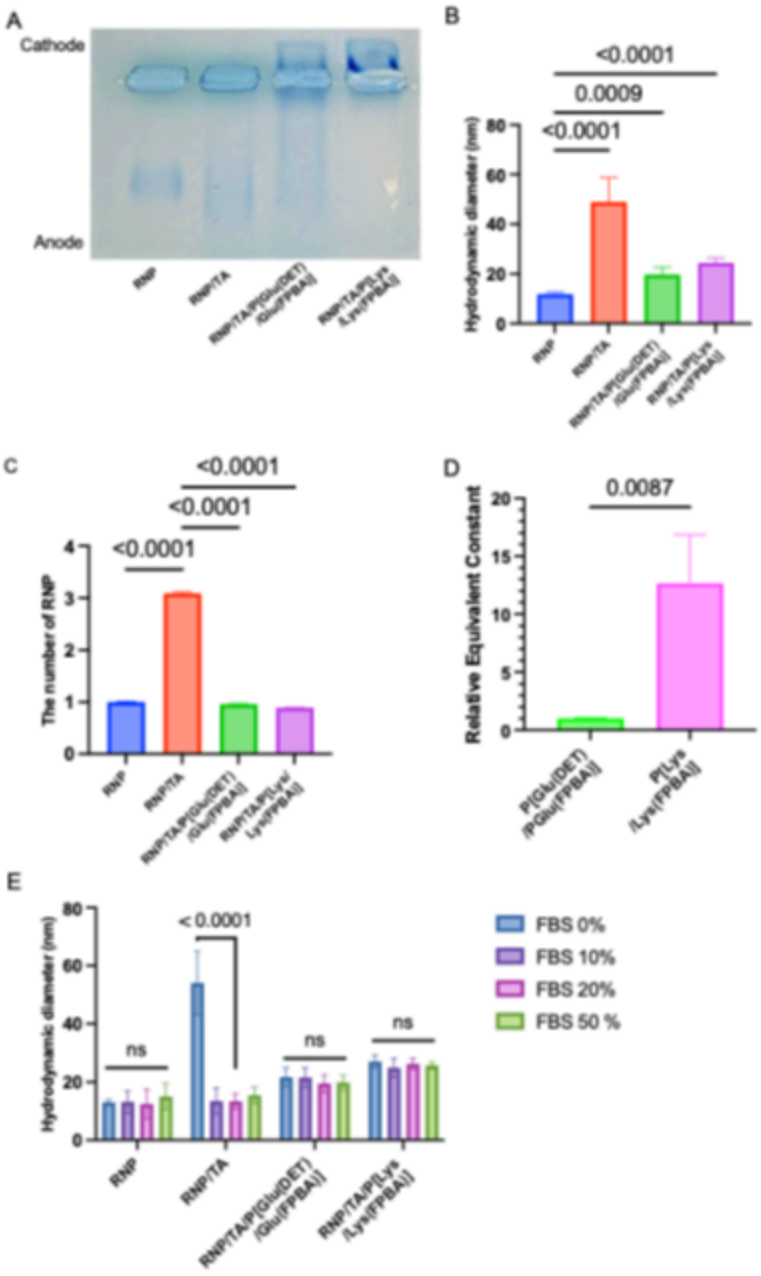

Figure 2

Characterization of RNP ternary complexes. (A) Native agarose gel electrophoresis of the ternary complexes. The gel was stained with Coomassie Brilliant Blue (CBB). (B) Hydrodynamic diameters and (C) the number of RNP molecules per complex determined by fluorescence correlation spectroscopy (FCS). (D) Relative apparent binding constants of the PBA-conjugated polymers with gallic acid, expressed relative to the apparent constant of P[Glu(DET)/Glu(FPBA)]. (E) Stability of the complexes in solutions containing fetal bovine serum (FBS), evaluated using GFP-tagged Cas9.Experimental conditions: [RNP] = 200 nM; [RNP]/[TA]/[PBA-conjugated polymer] molar ratio = 1/30/30.Data are presented as mean ± S.D. (n = 10 for B, C, and E; n = 3 for D). Statistical significance was analyzed using

one-way ANOVA followed by Tukey's multiple comparison test for (B), (C), and (E), and an unpaired t-test for (D).

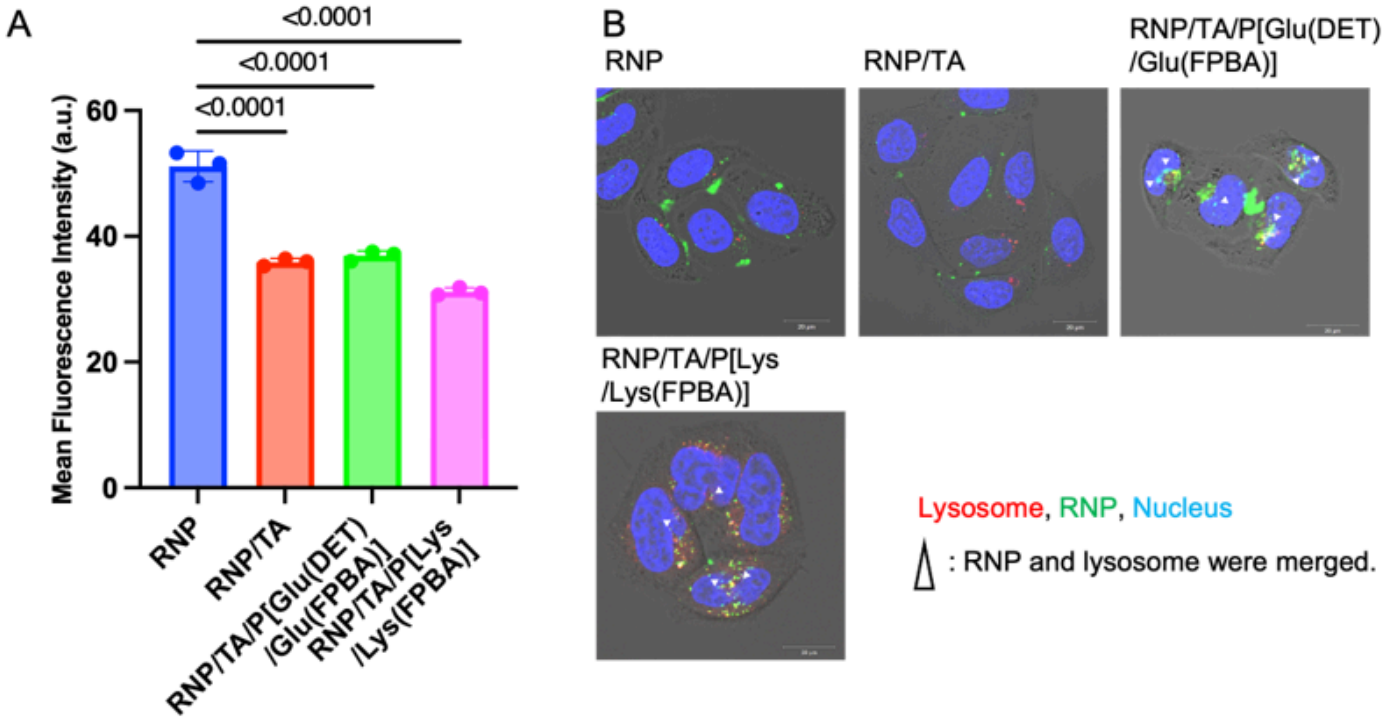

Figure 3

Subcellular distribution and cellular uptake of RNP samples. Cas9 with GFP tag was used. RNP concentrations: 60 nM, [RNP]/[TA]/[PBA-conjugated polymer]= 1/30/60. (A) Cellular uptake in HeLa-Luc cells evaluated by FCM. The cells were incubated with the samples for 24 h. Statistical analysis was performed using one-way ANOVA followed by Tukey's multiple comparison test. The results are expressed as mean ± S.D. (n = 3). (B) Subcellular distribution observed by CLSM. The samples were incubated with the samples for 24 h. RNP, Lysotracker Red DND-99, and nucleus are indicated as green, red, and blue respectively. Scale bar, 10 μm.

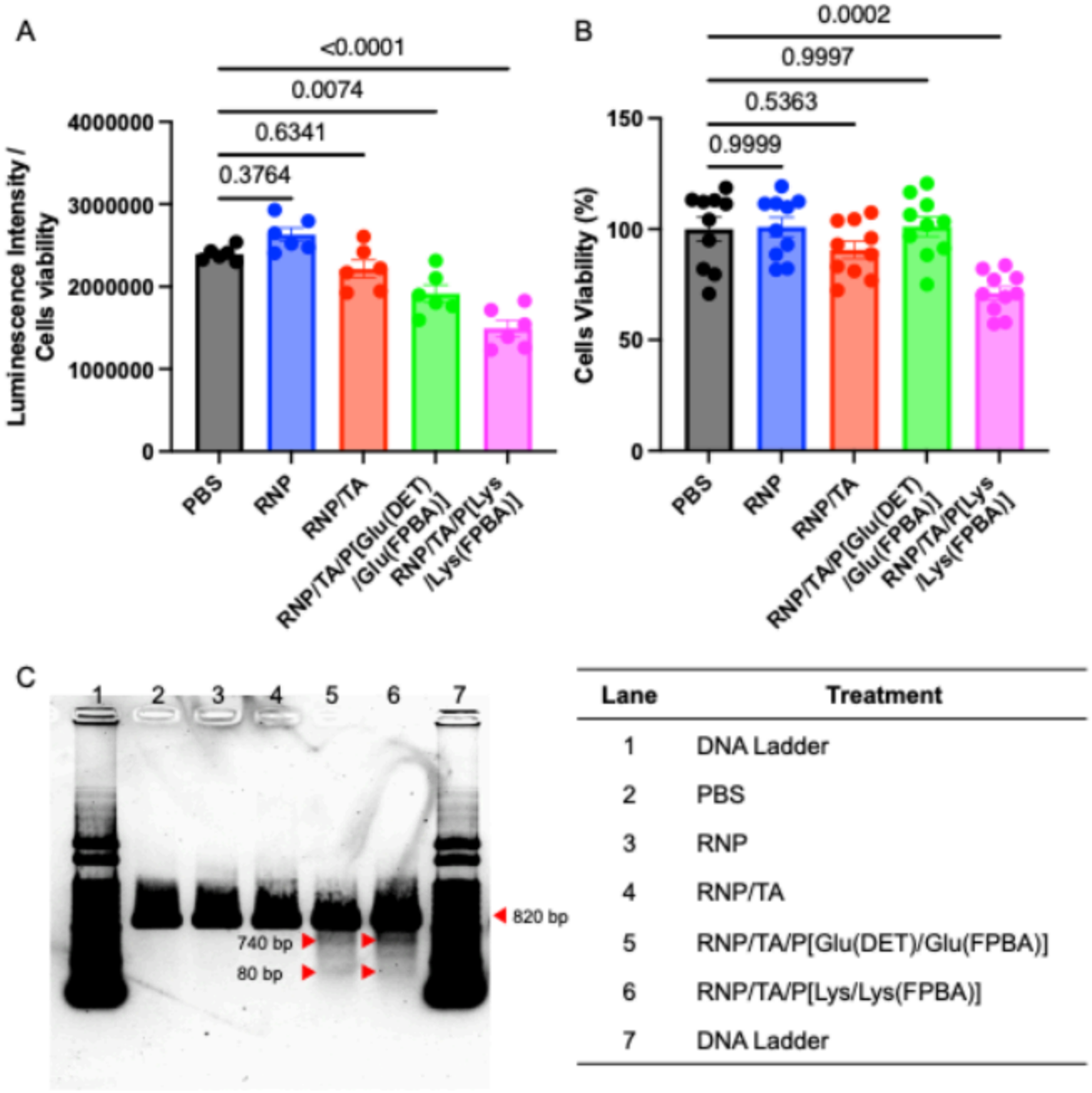

Lane	Treatment
1	DNA Ladder
2	PBS
3	RNP
4	RNP/TA
5	RNP/TA/P[Glu(DET)/Glu(FPBA)]
6	RNP/TA/P[Lys/Lys(FPBA)]
7	DNA Ladder

Figure 4

Luc gene editing by RNP ternary complex *in vitro*. RNP concentrations: 30 nM, [RNP]/[TA]/[PBA-conjugated polymer]= 1/30/60. (A) Luminescence intensity measurement. The cells were incubated with RNP samples for 72 h. The results are expressed as mean ± S.E.M. (n = 6) and normalized by cell's viability. (B) Cytotoxicity assay. The cells were incubated with RNP samples for 72 h. The results are expressed as mean ± S.D. (n = 10). (C) T7EI cleavage assay of DNA isolated from HeLa-Luc cells treated with various RNP samples. Red arrows indicate cleavage bands. This experiment was repeated three times independently with similar results. ANOVA with Tukey's multiple comparison test was used for statistical analysis in (A) and (B).

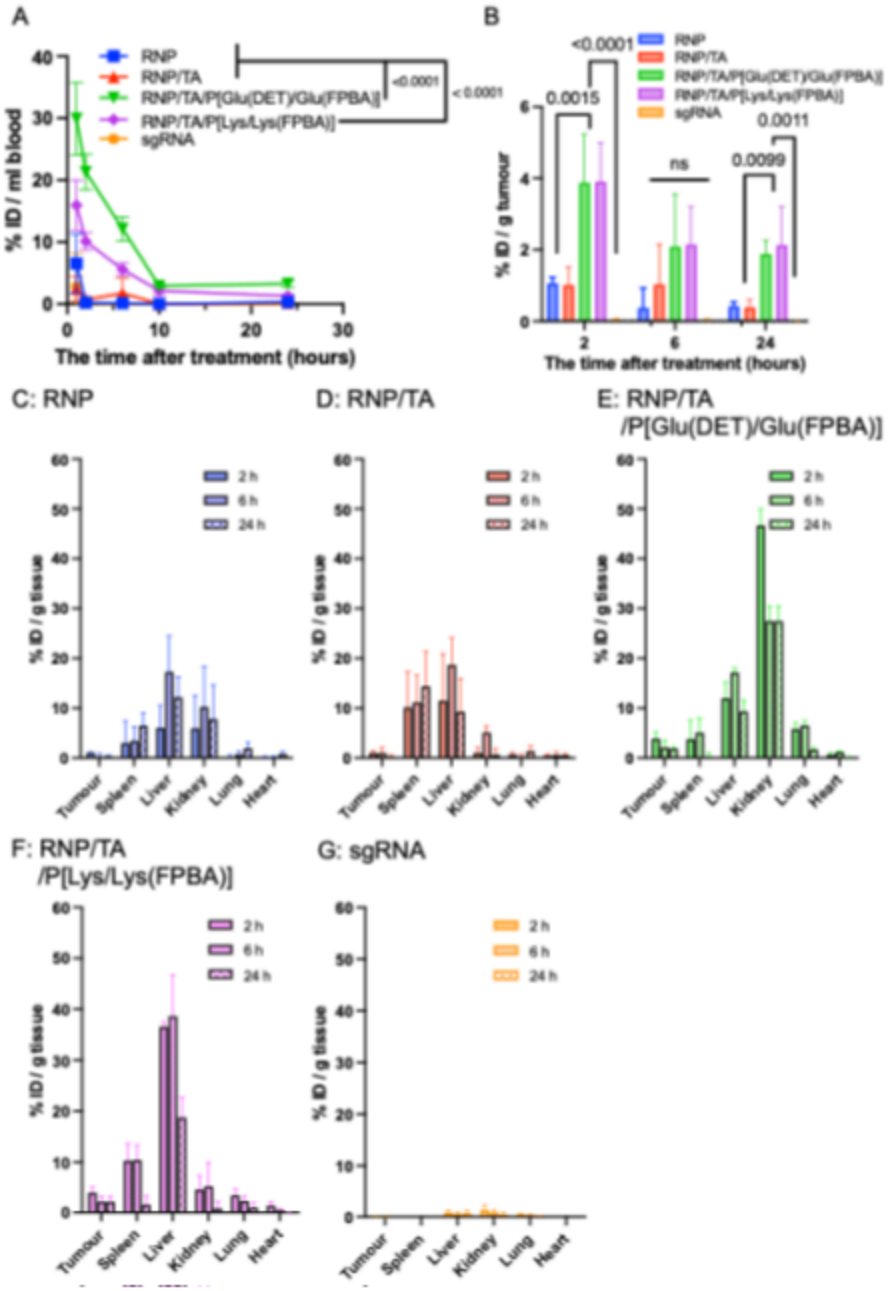

Figure 5

Biodistribution of intravenously injected RNP samples (32.0 μg of Cas9 and 6.4 μg) in subcutaneous HeLa-Luc tumor models. (A) Blood retention. The statistical difference at 2 hours post treatment was shown. (B) Tumor accumulation. (C-G) Biodistribution of (C) RNP, (D) RNP/TA, (E) RNP/TA/P[Glu(DET)/Glu(FPBA)], (F) RNP/TA/P[Lys/Lys(FPBA)] and (G) sgRNA. All the values were determined by Cy5 labelled sgRNA by fluorophotometer. The results are expressed as mean ± S.D. (n = 4). ANOVA with Tukey's multiple comparison test was used for statistical analysis in (A) and (B).

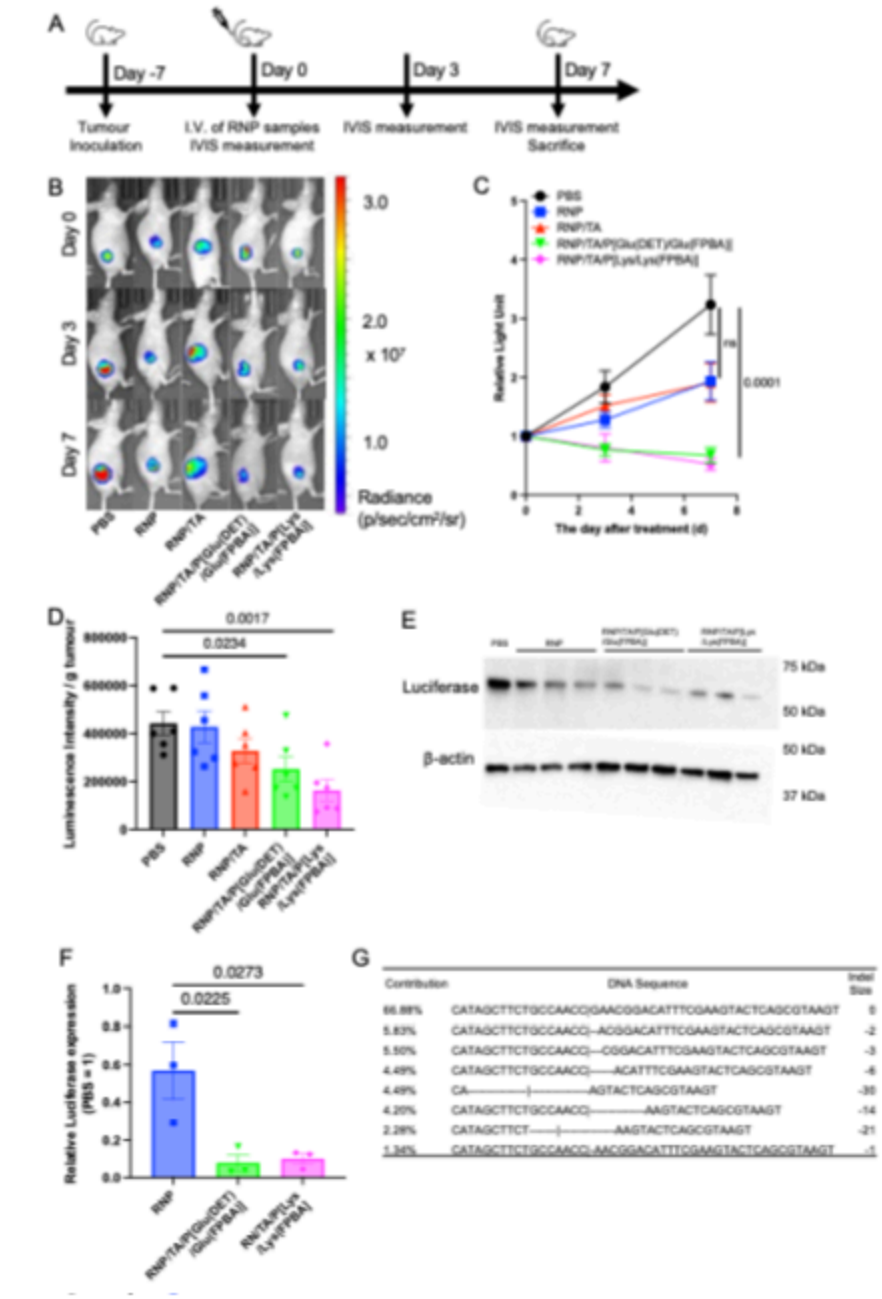

Figure 6

Luc gene editing by intravenously injected RNP samples (32.0 μg of Cas9 and 6.4 μg of sgRNA/mouse) in subcutaneous HeLa-Luc tumor models. (A) Scheme of the experiment. (B) The photos of mice received treatments taken by IVIS. (C) Luminescence intensity of the HeLa-Luc tumor. The value is normalized by the luminescence intensity on day 0. (D) Luminescence intensity of the lysed tumor. The intensity was normalized by the tumor weight. (E) Representative Western blot image showing Luc expression in Hela-Luc tumors treated with PBS, RNP, RNP/TA/P[Glu(DET)/Glu(FPBA)] and RNP/TA/P[Lys/Lys(FPBA)]. (F) Densitometric quantification of Luc levels normalized to Actin levels, and the relative values were then plotted against the PBS-treated group. (G) Sanger sequencing results of T-A cloning from HeLa-Luc tumor tissue after RNP/TA/P[Lys/Lys(FPBA)] treatment. The results are

expressed as mean ± S.E.M. (n = 5 or 6). ANOVA with Tukey's multiple comparison test was used in (C) and (F), and unpaired two-tailed t-tests with Welch correction was used in (D).

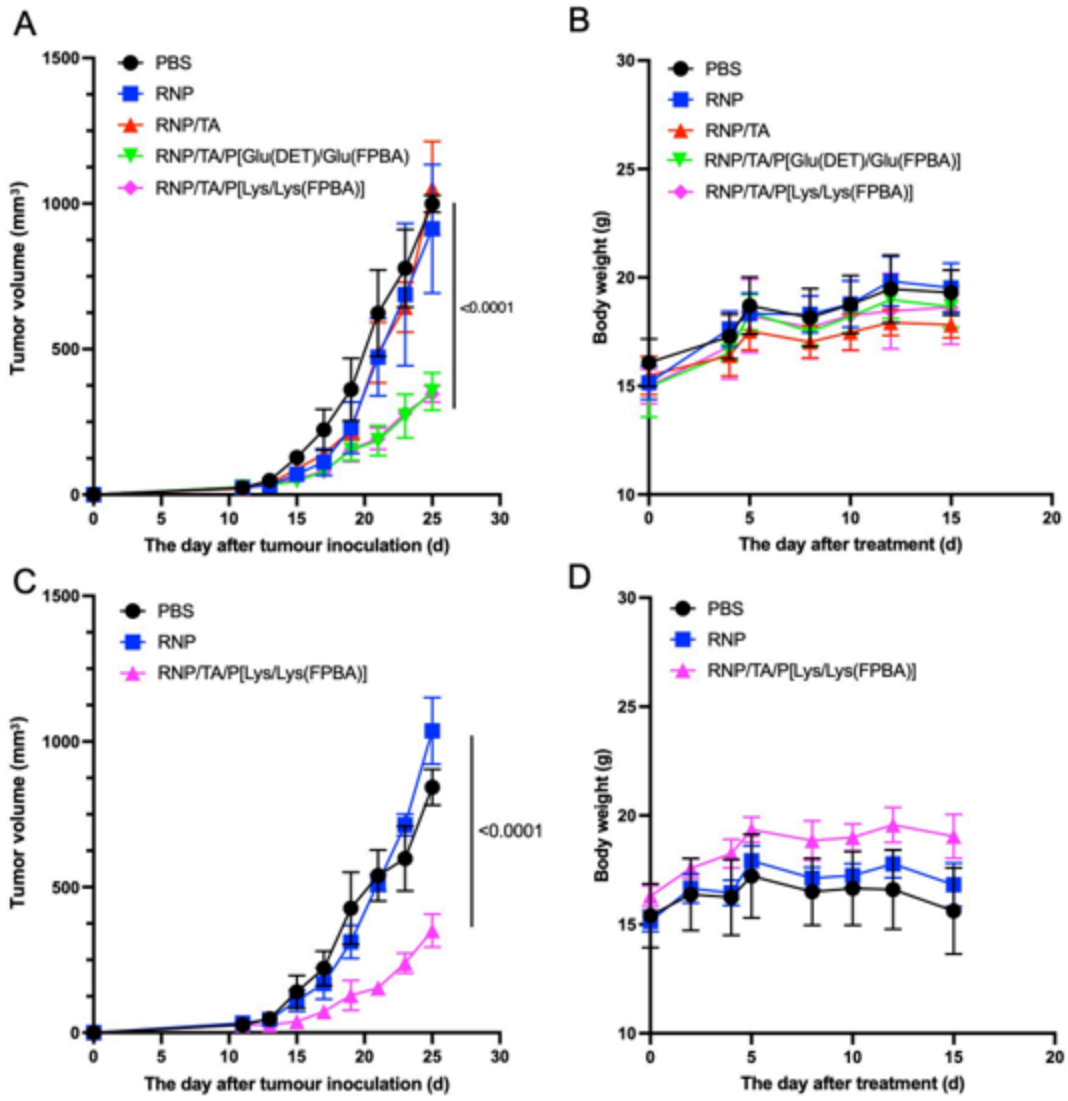

Figure 7

Anti-tumor study against HeLa-Luc and HCT116 subcutaneous tumor model mice. HeLa-Luc tumor cells were subcutaneously inoculated on day 0. PBS, RNP, RNP/TA, RNP/TA/P[Glu(DET)/Glu(FPBA)], RNP/TA/P[Lys/Lys(FPBA)] were administrated on day 11, day 13, and day 15. RNP was formed of Cas9 and sgRNA targeting PLK1. (A) The tumor growth curve and (B) body weight change of HeLa-Luc tumor model is shown. HCT116 tumor cells were subcutaneously inoculated on day 0, and PBS, RNP, RNP/TA/P[Lys/Lys(FPBA)] were administrated on day 11, day 13, and day 15. RNP was formed of Cas9 and sgRNA targeting $KRAS^{G13D}$. (C) The tumor growth curve and (D) body weight change of HCT116 tumor model. The results are expressed as mean ± S.E.M. ANOVA with Tukey's multiple comparison test was used for statistical analysis in both (A) and (C).

Supplementary Files

This is a list of supplementary files associated with this preprint. Click to download.

- JournalofNanobiosupplementmaterialTMv1.pdf
- JournalofNanobiosupplementalfileTMforgelandWB.pdf
- Graphicalabstract.png